DUAL POLARIMETRIC SAR DATA AT C-BAND FOR RICE CROP MAPPING USING DECISION TREE METHOD

4.1 INTRODUCTION

Rice (*Oryza sativa*) is one of the staple food grains in the world. India is one of the major rice-growing nations and accounts for one-fourth of the global rice area and produces approximately 125 million tons/year, with low yields of around 2.85 t/ha (Siddiq, 2000). India has undergone considerable economic development with intense urbanization and rapid spread in the population at the cost of reduced agricultural land. For such region, demand for higher rice production in decreased arable land is becoming a critical topic. A significant increase in the rice production is the only way to ensure the stable food production and security.

Access to timely, accurate and reliable data on rice crop distribution and its conditions provide information to decision-makers on sustainable food security, management of water resources and the environment. Satellite remote sensing provides a time saving and influential approach for monitoring agricultural area and other land cover features (Bastiaanssen et al., 2000; Thenkabail et al., 2007; Gumma et al., 2015, Jin et al., 2016; Mishra and Rai, 2016). Optical remote sensing is a viable approach to map rice growing areas effectively at regional and global levels because of its potential for large-area coverage and repeated observations (Fang, 1998; Xiao et al., 2004; Qin et al., 2015; Jin et al., 2016). Since most of the rice grows in rainy and cloudy regions, it is immensely difficult to attain cloud free optical images during critical rice growing seasons.

The emergence of spaceborne Synthetic Aperture Radar (SAR), with the advantages of all-weather, day and night imaging abilities, has drawn a lot of attention in remote sensing community for rice crop studies. The acquisition ability of SAR sensors at multiple frequencies and polarizations are ideal for mapping rice crop fields and understanding its backscattering response at various growth stages. In many studies, C-band polarimetric SAR images have been used effectively for mapping and monitoring of rice crop (Shao et al., 2001; Park and Chi, 2008; Nguyen et al., 2016; Kumar et al., 2016; Zeyada et al., 2016). In spite of the high potential of SAR data, its application has been restricted mainly by its availability. In last few decades, many spaceborne SAR systems have been launched like ERS- 1/2 in 1991 and 1995, JERS-1 in 1992, ENVISAT-ASAR in 2002, RADARSAT-1/2 in 1995 and 2007 and ALOS-PALSAR in 2006. But these sensors did not include the acquisition plan for regular regional observations. Therefore, SAR data provided by these sensors could not be used efficiently for mapping and monitoring of the rice crop in some regions. The launch of first Indian space-borne hybrid polarimetric SAR system Radar Imaging Satellite-1 (RISAT-1) by the Indian Space Research Organization (ISRO) in April 2012 brought more opportunities for the mapping and monitoring of rice crop (Gumma et al., 2015; Uppala et al., 2015). It carries a hybrid polarimetric SAR payload operating at C-band that supports right circular transmit and CoherenT Linear Receive (CTLR) mode as well to other standard modes. The imaging capability of RISAT-1 in HH, HV, VH, VV and circular polarizations ensured its broad aptness. Depending on different modes, RISAT-1 acquires data at various spatial resolution and swath (Misra et al., 2013; Valarmathi et al., 2013). The coupling of these noticeable features with regional observation plan makes RISAT-1 data very attractive for reliable image classification and appraisal of other agricultural practices

(Chakraborty et al., 2013; Kumar et al., 2016; Uppala et al., 2016). In some of the applications (classification cases), SAR images have better performance in comparison with optical images (Shao et al. 2001; Tan et al. 2007). Sometimes, SAR images cannot provide adequate mapping accuracy due to inherent speckle noise. The accuracy of rice crop mapping is also influenced by the similar backscattering responses of different land cover features (Okamoto and Kawashima, 1999).

The selection of a proper model or classification algorithm is always very vital for successful and accurate mapping of the rice crop and other land cover features. In spite of many studies in the field of SAR image classification; there are some specific limitations in each classification methods (Benediktsson et al., 1990; Mohammady et al., 2014). In addition to being widely used, supervised classification algorithms have some limitations. They are applied to the individual pixel level or image objects because of single discriminative nature. The selection of training data requires an extensive knowledge of the area and time. Also, supervised algorithms are incapable of identifying and characterizing unique classes not represented in training data. Unsupervised classification algorithms also have certain limitations. The natural grouping obtained by iterations in classifier does not essentially correspond adequately to desired informational classes. An analyst also has limited control over the classes selected during the classification process (Mishra et al., 2011). Thus to facilitate with more accurate results, it is beneficial to choose advanced classifiers inspired from machine learning theory. Therefore, a non-parametric approach that can train rapidly with its ability to handle large data sets from numeric and non-numeric sources is a good alternative. In recent years, self-learning Decision Tree (DT) classifiers have been used considerably for remote sensing image classification (Pal and Mather, 2003, Punia et al.,

2011; Aimaiti et al., 2016). The potential of DT classifiers for fruitful and accurate rice crop mapping is reported by many researchers (Choudhury and Chakraborty, 2006; Kumar et al., 2016; Nguyen et al., 2016; Zeyada et al., 2016). DT classifiers are computationally efficient and offer advantages such as flexibility, inherent simplicity, the capability to handle noisy and missing data (Friedl and Brodley, 1997; Aimaiti et al., 2016). Besides, it does not require probability distribution function of the data and is able to process large non-parametric datasets including both continuous and categorical data (Zambon et al., 2006). DT classifiers utilize recursive partitioning based on a variety of splitting rules to partition input dataset into categorical classes. So, DT classifier was adopted in this study for getting better accuracy in mapping rice crop and other land cover features.

In the context of above discussion, the objective of this study is to test the accuracy and validity of rice crop mapping using DT approach with medium resolution RISAT-1 image. Firstly, the backscattering response of rice crop and other land cover features for various polarizations were computed and examined. The DT classifier is then employed to map different land cover features, especially rice crop fields. The mapping accuracy of rice crop fields is finally validated with the rice crop fields extracted from Landsat 8-OLI image and ground reality in the study area. Limited comparative studies have been conducted using dual polarimetric RISAT-1 and multispectral Landsat-8 OLI images for mapping rice crop distribution. The approach used in this study is expected to provide an accurate and rapid mapping of rice cultivated regions. The method can also be exploited for cost-effective monitoring of rice crop and efficient yield prediction to ensure food production.

4.2 STUDY AREA

The study area for the present work is located in Varanasi district of Uttar Pradesh, India. It covers a total area of 35458.70 ha with center latitude 25°17′20.81″ N and longitude 82°58′39.10″ E (Figure 4.1). This land is very productive and agriculturally rich due to its location in the Indo-Gangetic plain. In this region, Rice is a dominant crop for the period of Kharif season. In addition to rice crop, the other crops like maize, sorghum, pigeon pea, pearl millet, etc. were also grown.
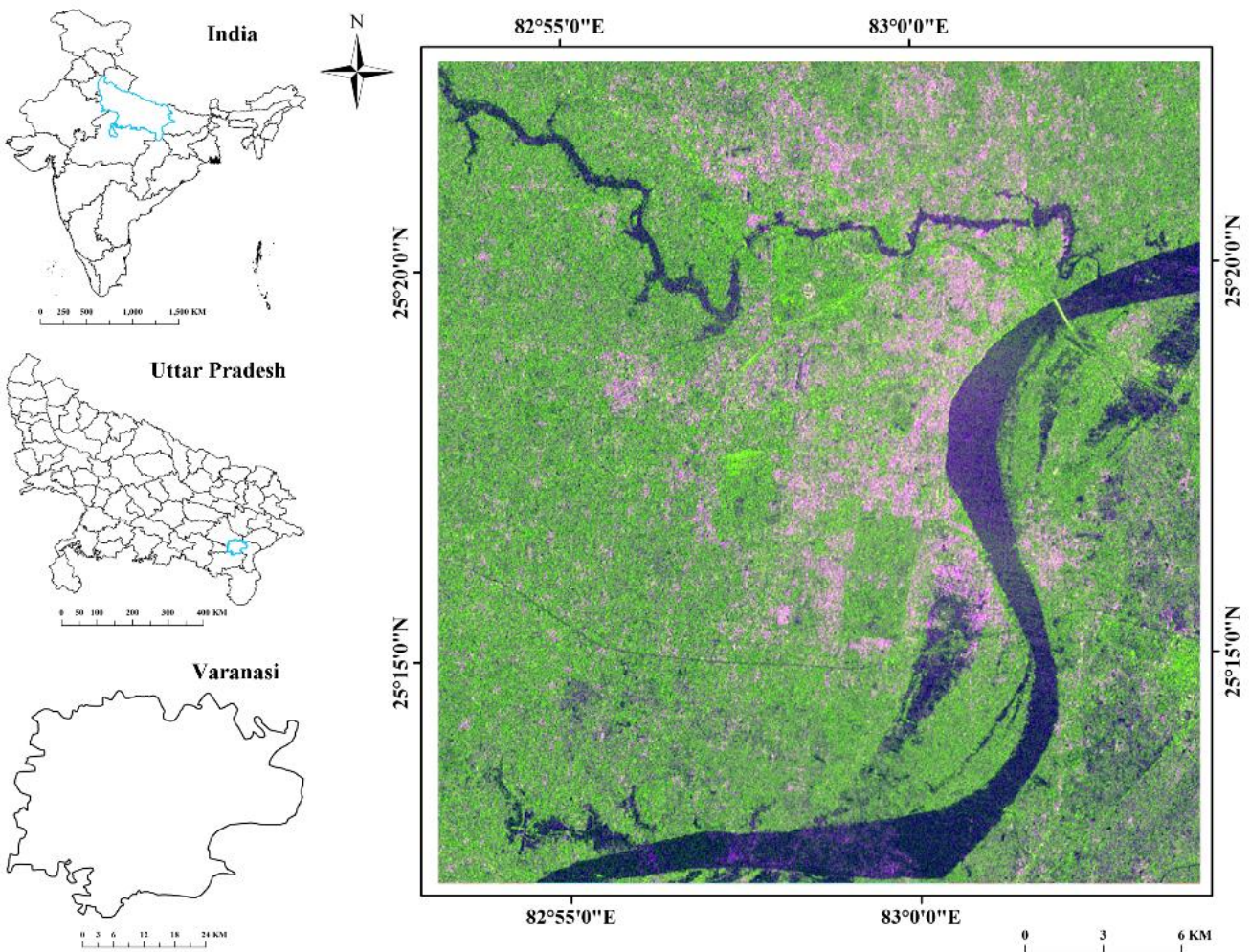

Figure 4.1 Location map of the study area as viewed on RISAT-1 Hybrid FCC image (*Red*-HH, *Green*-HV, *Blue*-HH-HV)

4.3 MATERIALS AND METHODOLOGY

4.3.1 Collection of satellite images and ground truth information

In this study, Medium-Resolution ScanSAR (MRS) mode RISAT-1 data at C-band with dual polarizations HH and HV was used to map the spatial distribution of rice crop. Only intensity images of HH and HV polarizations were available and used for the present study. The SAR data employed in this work was acquired on 3 September 2013. Alternatively, Landsat 8-OLI data was used to compare the output from RISAT-1 and evaluate the accuracy of rice crop mapping. The nearest available Landsat-8 OLI image was acquired on 6 September 2013. Only B2 to B7 of OLI sensor was used in this study. The specifications of RISAT-1 SAR and Landsat 8-OLI optical data are listed in Table 1.1. The study location was visited to collect ground truth information of target land cover features using a hand held GPS receiver.

4.3.2 Preprocessing of satellite images

4.3.2.1 RISAT-1 image

The RISAT-1 image was processed by ENVI-SARscape (v 5.1) image processing software. The RISAT-1 image was multi-looked 2 times in azimuth and 1 time in the range direction. The backscattering coefficient ($\sigma°$) was computed by using the Equation (2.1).

The speckles present in SAR images lead to degrading its quality. Therefore, it is requisite to reduce speckles before any further analysis of SAR images. In this study, different speckle filters namely mean, median, mode, Lee and Frost with window sizes of 3×3, 5×5, 7×7 and 9×9 were employed to reduce the speckles present in the RISAT-1 image.

The Speckle Suppression Index (SSI) was used to identify suitable filtering algorithm. This index is likely to be less than 1 and the lower SSI values indicate better performance of speckle filtering algorithm (Sheng and Xia, 1996). The equation of SSI is given as follows:

$$SSI = \frac{\sqrt{variance(I_f)}}{mean\ (I_f)} \times \frac{mean\ (I_o)}{\sqrt{variance\ (I_o)}} \qquad (4.1)$$

where I_f = filtered image and I_o = noisy image

The sigma naught ($\sigma°$) RISAT-1 image was geometrically corrected and spatially referenced to UTM projection system (Zone 44, North) with datum WGS 84 using georectified Landsat-8 OLI image using 15 equally distributed ground control points. A second-order polynomial equation was used, resulting in the RMSE of 1.06 pixels in both x and y directions.

It is valuable to use other composite images for the purpose of land cover classification (Miettinen and Liew, 2011; Wu et al., 2011). It can be produced by taking the ratio of HH and HV (Ratio = HH/HV) and the difference between HH and HV (Difference = HH-HV). The hybrid False Color Composite (FCC) image of HH, HV, and the difference image is shown in Figure 4.1.

4.3.2.1.1 Regions of interest for training and validation of classification algorithm

The present study was mainly focused on rice crop mapping. The samples were divided into four major land cover categories: rice, vegetation, built up and water bodies. The ROIs were primarily created with the help of field knowledge and high spatial resolution Google Earth images for training and validation of classification algorithm. The individual ROI polygons of land cover features were created in the middle of individual patches and well distributed over the study area. Training and validation ROIs were attained by random

selection of these ROIs. In total, 70% of the samples were randomly selected as the training samples, whereas 30% were used as the validation samples. The collection of training ROIs are depicted on Landsat 8-OLI image (Figure 4.2).
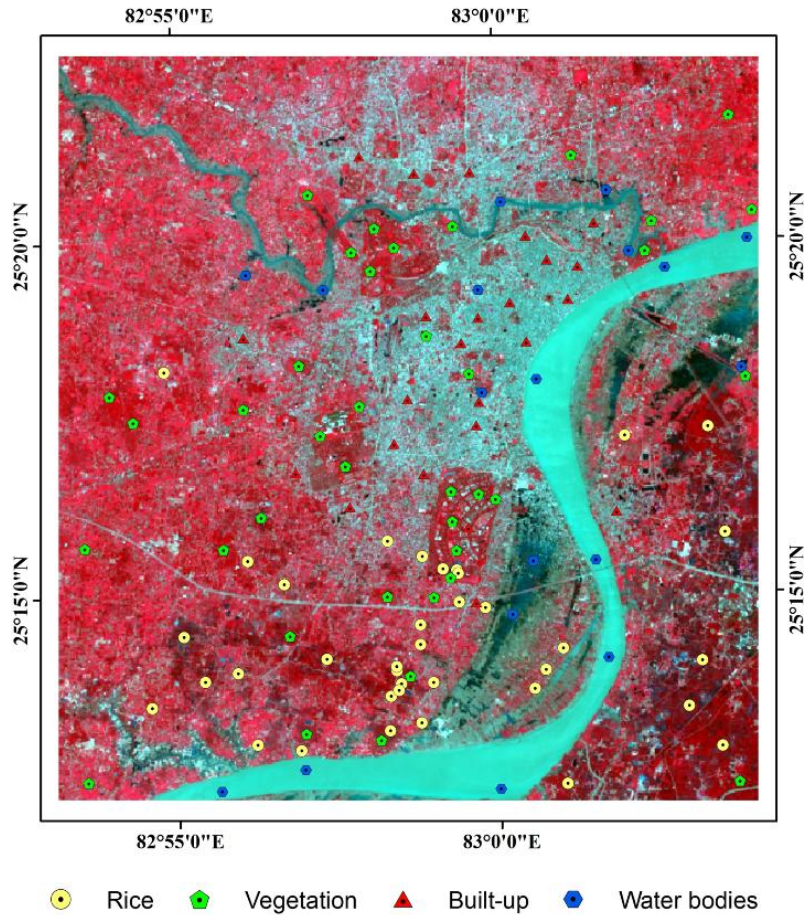

Figure 4.2 The ROIs used for training

4.3.2.1.2 Backscattering response analyses of rice crop and other land cover features

It is obligatory to understand the backscattering response of different land cover categories to achieve desired classification results. Microwave backscattering response is strongly affected by several factors such as polarization, frequency, surface roughness, geometric nature and dielectric properties of the target land cover features. For discriminating rice crop from other land cover features, the mean and Standard Deviation

(SD) of ROIs using the HH, HV, ratio and difference images were computed and are illustrated in Figure 4.3. The lowest backscatter values were shown by water bodies in both HH and HV polarizations because of specular reflection. Conversely, highest backscatter values were shown in the ratio and difference images. Therefore, water bodies can be identified effortlessly in respect to other land features. For HH polarization, rice crop backscatter value was found between vegetation and built up however; it was found close to each other at HV polarization. The variation in backscatter values of the rice crop and vegetation for difference (HH-HV) image was found higher than that of ratio (HH/HV) image. For ratio image, there was less variation in backscatter values of various land cover features in comparison to that of the difference image.
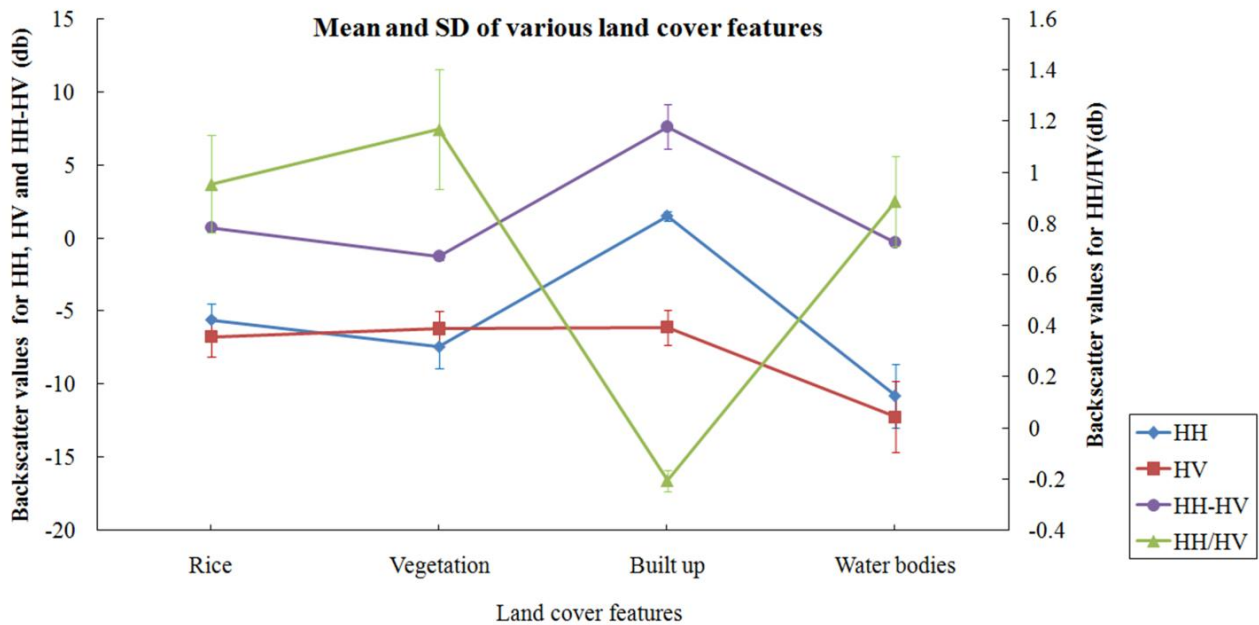

Figure 4.3 Comparison between statistical values of different land cover features using HH, HV, ratio, and difference images

Further, the histogram analysis of HH, HV, ratio and difference images were also performed for different land cover features to understand characteristics of various polarizations. Other than visual inspection of the histograms, a separability analysis was also

performed. The backscattering coefficients ($\sigma°$) of all polarizations for rice, vegetation, built up and water bodies were calculated. Since, each class signifies specific scattering behavior, decision boundaries are made from the knowledge acquired by the analysis of scattering behavior of each land cover features. In order to construct decision boundaries for the separation of different land cover features, a simple measure was calculated to compare the statistical separability of different land cover features by individual polarization data (Wu et al. 2011). The measure, known as separability index for class pair separation, is given as

$$S_{ij} = \frac{|\mu_i - \mu_j|}{\sigma_i + \sigma_j} \qquad\qquad (4.2)$$

where μ_i, μ_j and σ_i, σ_j are the means and standard deviations of classes i and j, respectively. Higher values of S_{ij} represent better separability between the two classes. The value of S_{ij}, lies between 0.8 and 1.5, signifies a useful feature for separation of two classes i and j. Values greater than 2.0 represent the feature for almost complete separation of class pairs.

4.3.2.2 Landsat 8-OLI image

Landsat 8-OLI image was first processed for atmospheric correction and converted into the top of atmosphere (TOA) reflectance in ENVI image processing software (*http://landsat.usgs.gov/ documents/Landsat8DataUsersHandbook.pdf*). The OLI bands were converted into the TOA planetary reflectance using reflectance rescaling coefficients given in the product specific metadata file (MTL file). The DN values were converted into TOA planetary reflectance for OLI image using the Equation given as:

$$\rho\lambda' = M_\rho Q_{cal} + A_\rho \qquad\qquad (4.3)$$

where $\rho\lambda'$ = TOA planetary reflectance (with no correction for solar angle), M_ρ = Band specific multiplicative rescaling factor from the metadata, A_ρ = Band specific additive

114

rescaling factor from the metadata, and Q_{cal} = the quantized and calibrated standard product pixel values (DN).

TOA reflectance with correction for the sun angle is the given by the Equation:

$$\rho\lambda = \frac{\rho\lambda'}{\sin(\theta_{SE})} \tag{4.4}$$

where $\rho\lambda$ = TOA planetary reflectance, $\rho\lambda'$ = TOA planetary reflectance (with no correction for solar angle), and θ_{SE} = the local sun elevation angle is given in the metadata file.

Since, different vegetation indices exhibit different characteristics for distinguishing rice crop from other land cover features. Two vegetation indices namely, normalized difference vegetation index (NDVI) (Tucker, 1979), enhanced vegetation index (EVI) (Huete et al., 2002; Xiao et al., 2004) and land surface water index (LSWI) (Xiao et al., 2004) were calculated using the TOA reflectance (ρ) from B1 (blue), B3 (red), B4 (NIR), and B5 (SWIR1) bands.

$$NDVI = \frac{\rho_{NIR} - \rho_{red}}{\rho_{NIR} + \rho_{red}} \tag{4.5}$$

$$EVI = G \times \frac{\rho_{NIR} - \rho_{red}}{\rho_{NIR} + C_1 \times \rho_{red} - C_2 \times \rho_{blue} + L} \tag{4.6}$$

$$LSWI = \frac{\rho_{NIR} - \rho_{SWIR\ 1}}{\rho_{NIR} + \rho_{SWIR\ 1}} \tag{4.7}$$

EVI requires blue band in combination with the red band to decrease atmospheric infectivity and also includes a soil background adjustment factor L. The values of coefficients C_1, C_2, and L were 6.0, 7.5, and 1.0, respectively. The value of a gain factor G was taken 2.5 (Huete et al., 2002).

The rice crop shows unique features during the ripening phase from late August to late September. Therefore, the indices LSWI, NDVI, and (NDVI + EVI)/2-LSWI can be used to

map rice crop fields (Jin et al. 2016). Firstly, homogenous and well distributed ROIs were visually interpreted and digitalized on the Landsat FCC image of LSWI, NDVI, and (NDVI + EVI)/2-LSWI for rice and other land cover features. A statistical separability index of different land cover features was calculated using equation (4.2).

4.3.3 QUEST DT algorithm for rice crop mapping

In this study, QUEST (*Quick, Unbiased, Efficient, Statistical Tree*) DT algorithm developed by Loh and Shih (1997) was used to delineate the rice cultivated areas from the dual polarimetric RISAT-1 image. For assessing the mapping accuracy of the dual polarimetric RISAT-1 image, the same classifier was used to classify Landsat-8 OLI image.

QUEST is a tree-structured binary split algorithm for classification and data mining (Chou et al., 2012). It is a nonparametric algorithm for automatic construction of decisions by creating splits without including additional user's interference. It yields a binary decision tree growing process including selection of a split variable, selection of a split point for the selected variable, and stopping. It also employs imputation instead of substitute splits to deal with missing values. QUEST is a computationally simple and rapid algorithm attributing an unbiased variable selection (Loh and Shih, 1997). This is accomplished by using two-step procedure for the generation of a DT. Initially, the split variable was selected followed by the split point calculation. It employs the ANalysis Of VAriance (ANOVA) *F*-statistic for selecting the variable and a modified Quadratic Discriminant Analysis (QDA) for split point selection from training data (Loh and Shih, 1997). In this type of analysis, the classification process was separated into two parts at each split (or node) because QUEST is assumed to be a binary decision tree. It provides the options between univariate and linear splitting rules. By using given training dataset, DT can be constructed for any statistical data.

116

4.3.3.1. Variable selection

The idea of QUEST was to reduce the bias by applying F-statistic and χ^2-statistic to estimate continuous and discrete features respectively. For each continuous feature X, an (ANOVA) F-statistic is performed to test if all the different classes of the dependent variable Y have the same mean of X, and calculate the p-value according to the F-statistics. For each discrete feature, perform χ^2-statistics of the independence of Y and X to calculate the p-value. It uses the following algorithm.

1. Find the feature with the smallest p-value and denote it by X*.

2. If p-value $< \alpha/M$, where $\alpha \in (0, 1)$ is a user-defined significance level and M is the total number of feature variables. X* is selected as the best split variable for the node.

3. If the p-value exceeds a user defined threshold, Levene's F-statistic for unequal variances is computed for each continuous variable X. The p-value is calculated for the test.

4. Find the feature with the smallest p-value and denote it by X**.

5. If smallest p-value $< \alpha/(M + M1)$, where M1 is the number of feature variable, then X** is selected as the split variable for the node. Otherwise, this node will not split (Loh and Shih, 1997).

4.3.3.2. Split point selection

QUEST is assumed to be a binary tree and the splits are done between two classes. So, it uses QDA to select a best split point. If there is a problem of classification to more than two classes, the classes are initially grouped into two superclasses by applying a two-means clustering algorithm (Hartigan and Wong, 1979) to the mean vectors for all the classes. In this algorithm, two most distant class means are considered as the cluster centers. If the class

means for all the classes are identical, then the most populous class becomes superclass *A* and the rest becomes superclass *B*. The procedure may be described as follows.

Suppose that a continuous variable *X* is selected to split a node N. By applying two-means clustering algorithm QDA estimates two classes (A, B) distributions with normal densities and determines the split point as an intersection point of two Gaussian curves, being a root of the equation

$$P(A|N)\frac{1}{\sqrt{2\pi S_A}}e^{-\frac{(x-\bar{x}_A)^2}{2S_A}} = P(B|N)\frac{1}{\sqrt{2\pi S_B}}e^{-\frac{(x-\bar{x}_B)^2}{2S_B}} \qquad (4.8)$$

where $\bar{x}_A$ and S_A denote the mean and standard deviation of superclass A. Similarly, $\bar{x}_B$ and S_B denotes the mean and standard deviation of superclass B. The parameters (mean and standard deviation) of normal densities are calculated from the samples. After transformation of equation (1), a quadratic equation is obtained as:

$$ax^2 + bx + c = 0 \qquad (4.9)$$

where

$$a = S_A{}^2 - S_B{}^2 \qquad (4.10)$$

$$b = 2\big(\bar{x}_A S_B{}^2 - \bar{x}_B S_A{}^2\big) \qquad (4.11)$$

$$c = (\bar{x}_B S_A)^2 - (\bar{x}_A S_B)^2 + 2S_A{}^2 S_B{}^2 \log\frac{n_A S_B}{n_B S_A} \qquad (4.12)$$

One of the two roots that are closer to $\bar{x}_A$ is considered as the split point provided this yields two non-empty nodes.

The QUEST algorithm was implemented in the software add-on Rule Gen 1.02 running in ENVI 5.1 image processing environment. An unbiased statistical test for variable selection and a QDA for split threshold selection were applied to run the model. Here univariant splitting rule was taken into consideration and cross validation (CV) method was used for

tree pruning. The QUEST algorithm provides other options such as standard errors (SEs), alpha value, minimum node size, variable selection method, output Pstricks tree, and so on. The ROIs created from images were used to train the algorithm and to derive a final rice crop map. The working flow chart for rice crop mapping is shown in Figure 4.4.
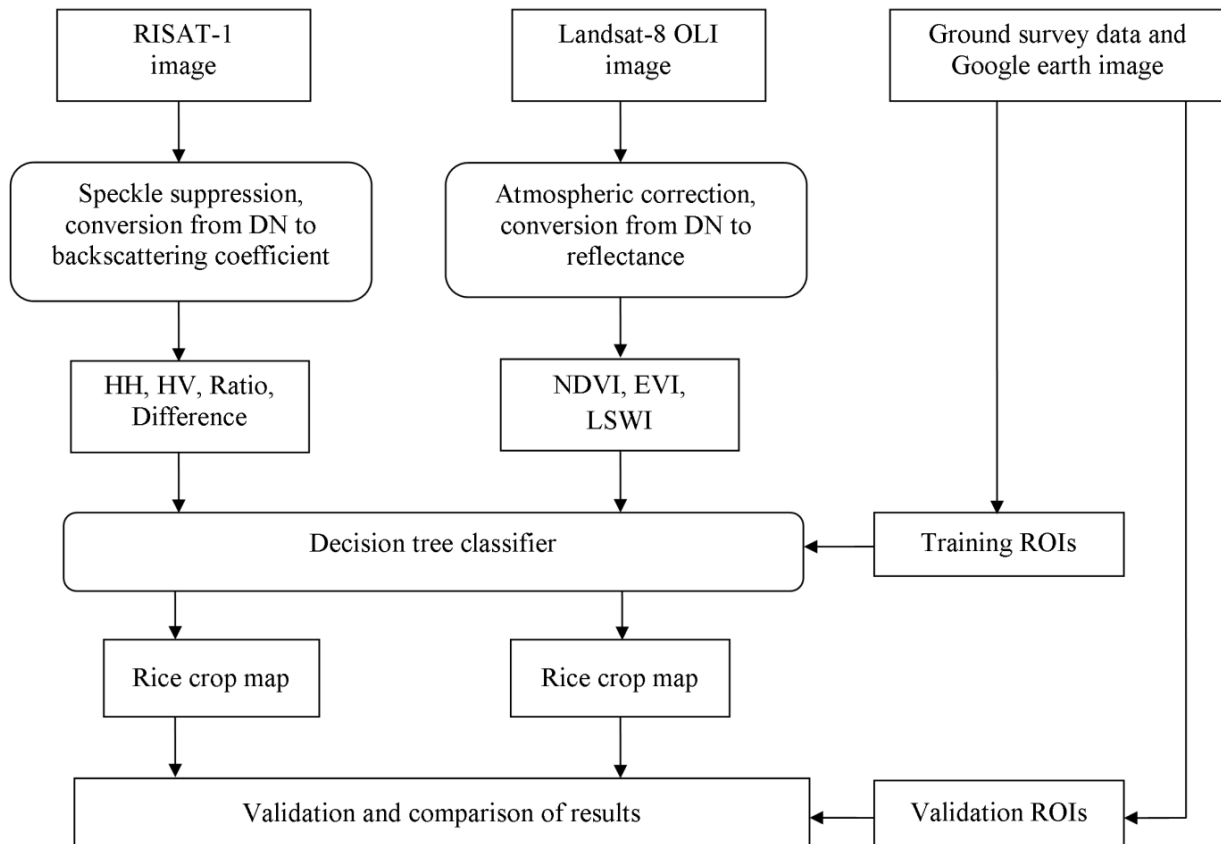

Figure 4.4 The working flow chart for rice crop mapping

4.3.4 Assessment of classification accuracy

A confusion matrix was calculated to appraise the resultant maps of land cover features. It is a widely used approach for evaluating the accuracy of the resultant map by comparing it with the ground truth data. Randomly selected 30% of the field data for each class were used as validation samples. The accuracy assessment parameters like overall classification accuracy (OCA), UA, PA, K_C and F- score was computed.

A preliminary use of ROC curves in machine learning for evaluation and comparison of the algorithm was demonstrated (Spackman, 1989). The performance evaluation using simple classification accuracy measures is often realized as a poor metric. Therefore, in recent years, ROC curves have gained attention in machine learning community for organizing and visualizing the performance of classifiers (Fawcett, 2006). It is derived from signal detection theory and has been broadly used in several studies to appraise the accuracy of classified products and other applications (Bradley 2009; Alatorre et al., 2011; Kumar and Krishna, 2016). In a ROC curve, the area under the curve (AUC) is used as a measure of the accuracy of a prediction model. According to Kumar and Krishna (2016), the AUC and prediction accuracy relation can be categorized into poor (0.5–0.6), average (0.6–0.7), good (0.7–0.8), very good (0.8–0.9) and excellent (0.9–1). ROC curve was used to compare the rate of rice crop detection versus false positive rate (pixels identified as rice that did not contain rice).

The ROC curve for classification is determined by calculating the sensitivity (true positives) and 1-specificity (false positives) given by Equations (4.13) and (4.14) respectively. The overall reliability is another common statistics and given by Equation (4.15).

$$\text{Sensitivity} = \frac{a}{(a + c)} \tag{4.13}$$

$$1 - \text{specificity} = \frac{b}{(b + d)} \tag{4.14}$$

$$\text{Reliability} = \frac{b + d}{(a + b + c + d)} \tag{4.15}$$

where a represents true positives, d represents true negatives, b represents false positives, and c represents false negatives (Table 4.1).

Table 4.1 A confusion matrix showing the proportion (or number) of pixels in observed map versus predicted map. Here 'a' represents true positives, d represents true negatives, b represents false positives, and c represents false negatives

		Observed		
		Rice	Non-rice	Total
Predicted	Rice	a	b	a+b
	Non-rice	c	d	c+d
	Total	a+c	b+d	a+b+c+d

4.4 RESULTS AND DISCUSSION

The mean and Standard Deviation (SD) values of the raw and speckle filtered images with different window sizes are listed in Tables 4.2 and 4.3 respectively. The output values of SSI for the median filter with a kernel size of 9×9 provided the best result at HH polarization, while the mean filter with kernel size of 9×9 was found best for HV polarization. These filtered images were used for further analysis and classification. The histograms of HH, HV, ratio and difference images were analyzed for the four land cover features and are shown in Figure 4.5. In HH image, all the land cover features are well separable while they were overlapped for HV image especially for rice and vegetation class. At the same time, rice crop has high backscatter value for difference image and is separable from vegetation. Therefore, taking into account the HH, ratio and difference backscatter values, rice crop can be separated from vegetation and other land cover features.

Table 4.2 Mean and SD for raw and filtered images of HH polarization

	Window size	Mean	SD	Mean/SD	SSI
		HH polarization			
Noisy image		2955.49	2631.48	1.12	
Filter					
	3x3	2954.92	1902.79	1.55	0.72
	5x5	2954.64	1792.25	1.65	0.68
Mean	7x7	2954.43	1719.17	1.72	0.65
	9x9	2954.33	1665.33	1.77	0.63
	3x3	2703.83	1626.14	1.66	0.68
	5x5	2663.05	1476.79	1.80	0.62
Median	7x7	2636.11	1387.45	1.90	0.59
	9x9	2615.87	1321.70	1.98	0.56
	3x3	2468.66	1478.75	1.67	0.67
	5x5	2408.78	1344.04	1.79	0.63
Mode	7x7	2366.27	1252.14	1.89	0.59
	9x9	2337.48	1192.09	1.96	0.57
	3x3	2951.41	2204.20	1.34	0.84
	5x5	2952.02	2171.12	1.36	0.83
Frost	7x7	2953.92	2174.37	1.36	0.83
	9x9	2954.77	2180.56	1.36	0.83
	3x3	2936.50	2110.64	1.39	0.81
	5x5	2946.07	2071.14	1.42	0.79
Lee	7x7	2957.02	2044.46	1.45	0.78
	9x9	2960.75	2020.11	1.47	0.77

Table 4.3 Mean and SD for raw and filtered images of HV polarization

|	Window size	Mean	SD	Mean/SD	SSI
		HV polarization			
Noisy image		2909.32	1137.27	2.56	
Filter					
Mean	3x3	2909.68	698.77	4.16	0.61
	5x5	2909.77	647.46	4.49	0.57
	7x7	2909.83	618.85	4.70	0.54
	9x9	2909.91	599.52	4.85	0.53
Median	3x3	2821.45	696.30	4.05	0.63
	5x5	2810.74	639.61	4.39	0.58
	7x7	2804.79	609.37	4.60	0.56
	9x9	2800.84	589.92	4.75	0.54
Mode	3x3	2706.33	800.73	3.38	0.76
	5x5	2691.97	771.07	3.49	0.73
	7x7	2679.32	751.00	3.57	0.72
	9x9	2669.59	737.21	3.62	0.71
Frost	3x3	2908.17	810.08	3.59	0.71
	5x5	2908.61	771.61	3.77	0.68
	7x7	2909.09	761.51	3.82	0.67
	9x9	2929.20	758.94	3.83	0.67
Lee	3x3	2895.55	1073.99	2.70	0.95
	5x5	2907.45	1076.18	2.70	0.95
	7x7	2915.36	1062.78	2.74	0.93
	9x9	2918.27	1046.48	2.79	0.92
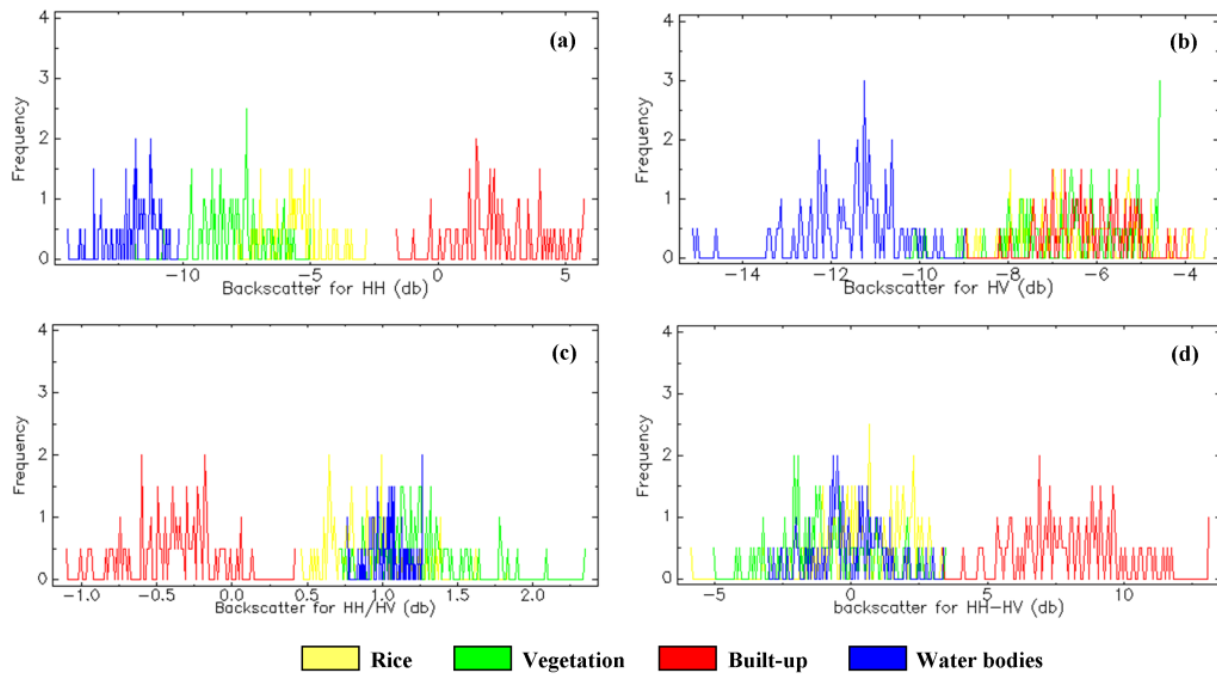
Figure 4.5 Comparison between histograms of different land cover features in four images: (a) HH polarization, (b) HV polarization, (c) ratio image, and (d) difference image

The separability index (S_{ij}) emphasized the usability of HH and difference image due to having its high values between rice and other land cover features for the discrimination of rice crop. Figure 4.6 shows separability index for all the defined class pairs using RISAT-1 image. It indicates that HH and difference polarization images are good and useful features for separation of rice and vegetation followed by HH/HV polarization ratio. However, HV was found worst feature for the separation of rice and vegetation. Other class pairs exhibited almost complete separation for all polarization images. The values of separability index were found to be useful for all class pairs using the training ROIs collected from the Landsat 8-OLI FCC image and are shown in Figure 4.7. It shows that NDVI and (NDVI + EVI)/2 - LSWI were found to be useful features for the separation of rice and vegetation classes followed by LSWI. Other class pairs exhibited almost complete separation for all indices.
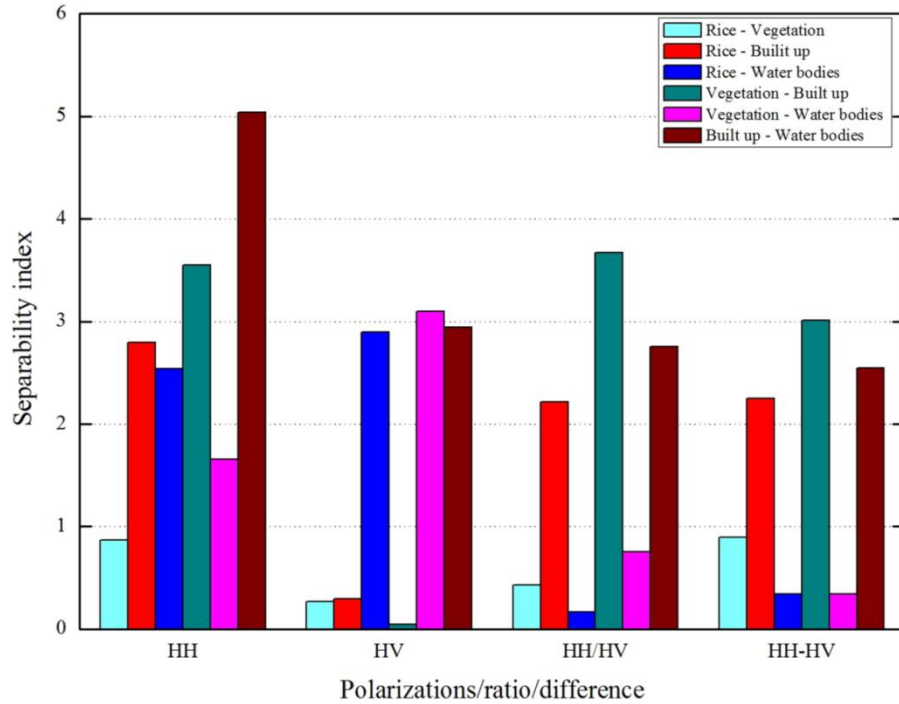
124

Figure 4.6 Separability index for class pair separation by various features (HH, HV, ratio, and difference) using RISAT-1 image
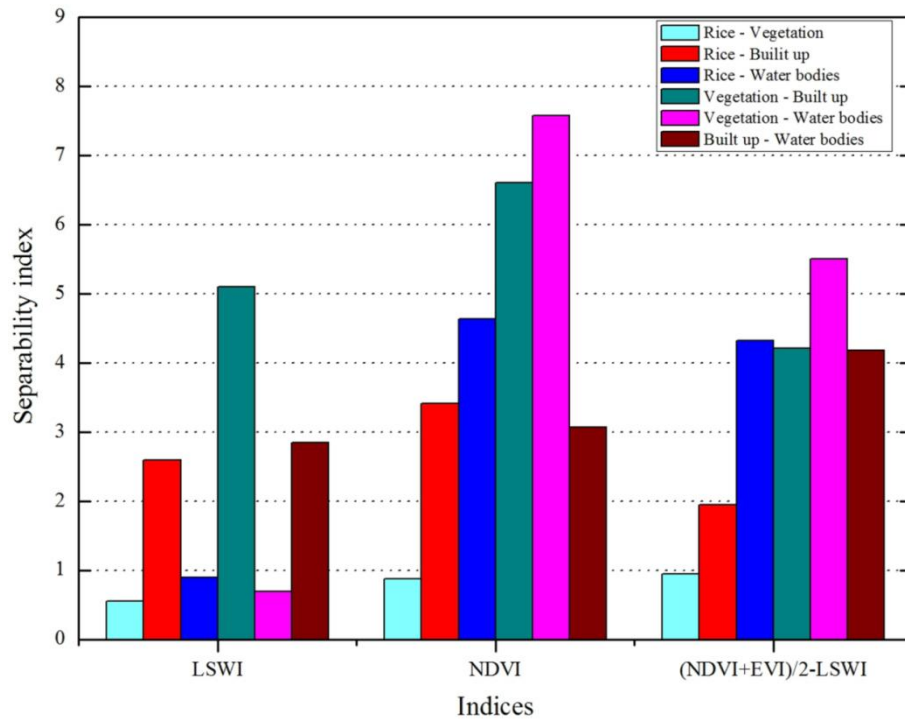

Figure 4.7 Separability index for class pair separation by various features (LSWI, NDVI, and (NDVI + EVI)/2 - LSWI) using Landsat 8-OLI image

4.4.1 Rice crop maps using RISAT-1 and Landsat 8-OLI images

The outputs of QUEST classification algorithm using RISAT-1 and Landsat 8-OLI images are illustrated in Figure 4.8. The OCA of Landsat 8-OLI and RISAT-1 MRS data was estimated as 91.29% and 88.57% with kappa coefficient 0.884 and 0.874 respectively. The PA, UA and F-score calculated relative to QUEST DT algorithm are shown in Table 4.4. Rice cropped area was estimated to be 7885.10 and 8555.92 ha from Landsat 8-OLI and RISAT-1 dual polarimetric images, respectively. However, the rice cropped area was overestimated using RISAT-1 image due to similar backscattering response of the shrubs present on the field bunds boundaries. Also, the built-up class mixes with vegetation class due to having volume scattering mechanism in RISAT-1 image. It may be one of the reasons that built-up class was underestimated using RISAT-1 in comparison to that of Landsat 8-OLI image. The spatial distribution of land cover features for both the classified outputs is presented in Table 4.5.
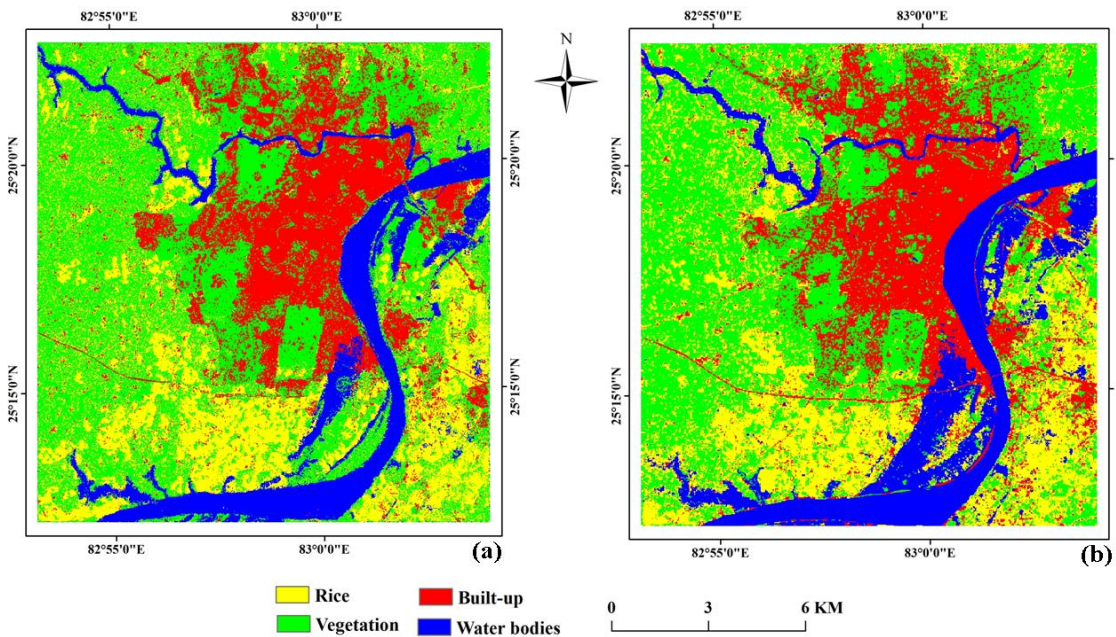

Figure 4.8 DT algorithm based classified maps of (a) RISAT-1, and (b) Landsat 8-OLI images

126

Table 4.4 The classification accuracies of Landsat 8-OLI and RISAT-1images

Land cover feature	Landsat-8 OLI			RISAT-1		
	PA (%)	UA (%)	F-score (%)	PA (%)	UA (%)	F-score (%)
Rice	88.36	86.53	87.43	85.26	83.94	84.60
Vegetation	91.93	89.70	89.02	86.83	87.88	86.55
Built-up	93.99	96.09	96.09	93.85	93.85	89.35
Water bodies	91.09	92.93	90.59	88.44	88.89	87.04
OCA (%)		91.29			88.57	
Kc		0.884			0.874	

Table 4.5 Area statistics comparison of land cover features

Land cover feature	Area (ha)	
	RISAT-1	Landsat 8-OLI
Rice	8555.92	7885.10
Vegetation	15551.64	14386.04
Built-up	6934.94	7646.74
Water bodies	4416.20	5540.81
Total	35458.70	35458.70

4.4.2 Validation of rice crop maps using ROC curves

The ROC curves were used to assess the performance of QUEST classification in rice crop mapping. Since the main focus of the present study was to map rice crop area using RISAT-1 and Landsat 8-OLI images, the rice and non-rice areas were identified with the help of ground truth information collected through field visit and Google earth images. The rice crop maps were finally validated with the available ground truth information. In the ROC curve, 1-specificity (false positive rate) on the X-axis was plotted against sensitivity (true positive rate) on the Y-axis. A higher sensitivity signifies several true positives or correct

predictions, while a higher specificity indicates many false positives. The ROC curves for the rice crop area with RISAT-1and Landsat 8-OLI images are shown in Figure 4.9 (a, b). For the RISAT-1 image, the ROC statistic or AUC was 0.858, which corresponds to the prediction accuracy of 85.8% (Figure 4.9 (a)), while for Landsat 8-OLI image, the ROC statistic or AUC was found to be 0.881, which corresponds to the prediction accuracy of 88.1% (Figure 4.9 (b)). Hence, the map produced by QUEST method exhibited good result in predicting the cultivated rice area in a part of Varanasi district of Uttar Pradesh, India.

The outcomes of this study established the effectiveness of the method proposed for the rice crop mapping. Also, the method can be used profoundly for cost-effective monitoring of rice crop.
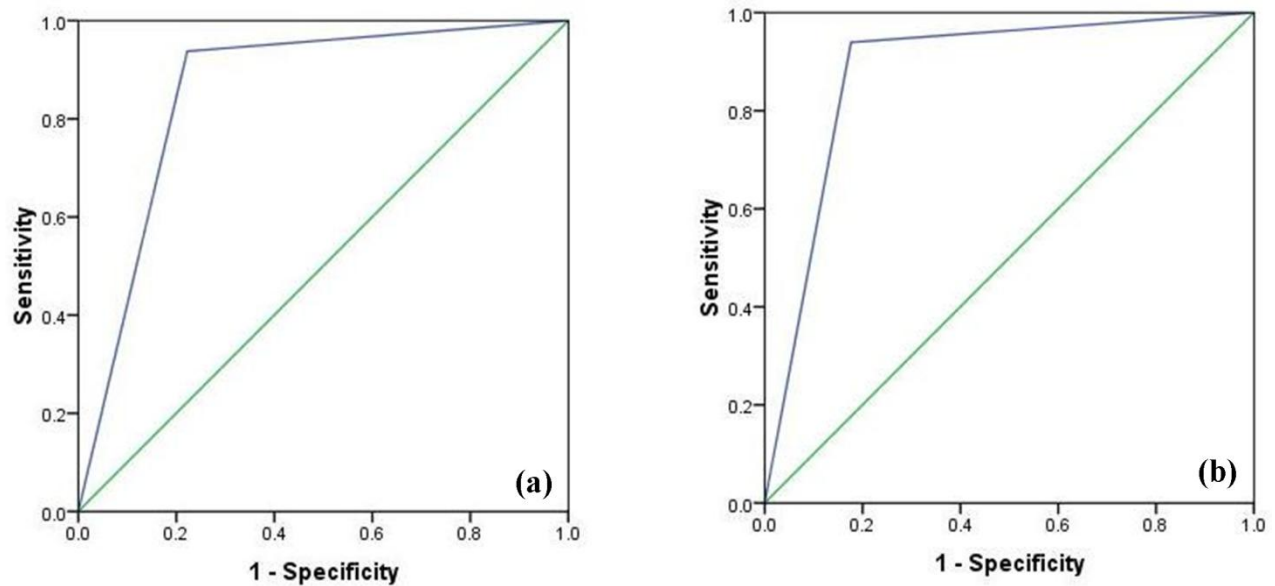

Figure 4.9 The ROC curves for the rice crop area mapping using (a) RISAT-1, and (b) Landsat 8-OLI images

4.5 CONCLUSION

The present study investigated the feasibility of using single date dual polarimetric RISAT-1 data for discrimination of rice crop from the other land cover features using QUEST classifier. The major findings of this work were that (i) the image acquired during

the growing stage reveals an optimal difference between the backscattering response of rice and other land cover features (ii) the composite image of the ratio (HH/HV) and difference (HH-HV) enhances backscatter separability between rice and other land cover features and (iii) with the optimal polarization combination based on the backscattering response behavior, a QUEST DT algorithm effectively identified rice crop areas with high accuracy.

Moreover, the results showed that HH along with HH/HV and HH-HV was the best polarization combination with accuracy up to 88.57% for mapping the spatial distribution of rice crop. An excellent spatial agreement of almost 90% was observed between rice crop areas derived from dual polarimetric RISAT-1 and multispectral Landsat 8-OLI images. Rice crop areas were estimated to be 7885.10 and 8555.92 ha from Landsat 8-OLI and RISAT-1 images respectively. In summary, this work demonstrated that dual polarimetric MRS mode data from the newly launched RISAT-1 satellite could be a promising source for rice crop discrimination and mapping. In future studies, identification and discrimination of rice crop at different growth stages can be used to improve the accuracy. Additionally, the study of the relationship between rice crop parameters and polarimetric parameters can help to develop a method for yield estimation.